# BAFF/BLyS Receptor 3 Comprises a Minimal TNF Receptor-like Module That Encodes a Highly Focused Ligand-Binding Site‡

Nathaniel C. Gordon,⊥,§ Borlan Pan,⊥,§ Sarah G. Hymowitz,⊥ JianPing Yin,⊥ Robert F. Kelley,⊥ Andrea G. Cochran,⊥ Minhong Yan,∥ Vishva M. Dixit,∥ Wayne J. Fairbrother,⊥ and Melissa A. Starovasnik*,⊥

*Departments of Protein Engineering and Molecular Oncology, Genentech, Inc., One DNA Way, South San Francisco, California 94080*

*Received January 7, 2003*

ABSTRACT: BAFF/BLyS, a member of the tumor necrosis family (TNF) superfamily of ligands, is a crucial survival factor for B cells. BAFF binds three receptors, TACI, BCMA, and BR3, with signaling through BR3 being essential for promoting B cell function. Typical TNF receptor (TNFR) family members bind their cognate ligands through interactions with two cysteine-rich domains (CRDs). However, the extracellular domain (ECD) of BR3 consists of only a partial CRD, with cysteine spacing distinct from other modules described previously. Herein, we report the solution structure of the BR3 ECD. A core region of only 19 residues adopts a stable structure in solution. The BR3 fold is analogous to the first half of a canonical TNFR CRD but is stabilized by an additional noncanonical disulfide bond. BAFF-binding determinants were identified by shotgun alanine-scanning mutagenesis of the BR3 ECD expressed on phage. Several of the key BAFF-binding residues are presented from a $\beta$-turn that we have shown previously to be sufficient for ligand binding when transferred to a structured $\beta$-hairpin scaffold [Kayagaki, N., Yan, M., Seshasayee, D., Wang, H., Lee, W., French, D. M., Grewal, I. S., Cochran, A. G., Gordon, N. C., Yin, J., Starovasnik, M. A, and Dixit, V. M. (2002) *Immunity 10*, 515−524]. Outside of the turn, mutagenesis identifies additional hydrophobic contacts that enhance the BAFF−BR3 interaction. The crystal structure of the minimal hairpin peptide, bhpBR3, in complex with BAFF reveals intimate packing of the six-residue BR3 turn into a cavity on the ligand surface. Thus, BR3 binds BAFF through a highly focused interaction site, unprecedented in the TNFR family.

BAFF (also known as BLyS, TALL-1, THANK, TNFSF13B, or zTNF4) is a member of the TNF[1] ligand superfamily that is essential for B cell survival and maturation (reviewed in ref *1*). BAFF overexpression in transgenic mice leads to B cell hyperplasia and development of severe autoimmune disease (*2*−*4*). BAFF levels are elevated in human patients with a variety of autoimmune disorders, such as systemic lupus erythematosus, rheumatoid arthritis, and Sjögren's syndrome (*5*−*7*). Furthermore, BAFF levels correlate with disease severity, suggesting that BAFF may play a direct role in the pathogenesis of these illnesses. BAFF acts on B cells by binding to three members of the TNF receptor superfamily, TACI, BCMA, and BR3 (also known as BAFF-R) (*3*, *8*−*10*). Of the three, only BR3 is specific for BAFF; the other two also bind the related TNF family member, APRIL. Comparison of the phenotypes of BAFF and receptor knockout or mutant mice indicates that signaling through BR3 mediates the B cell survival functions of BAFF (*8*, *9*, *11*). In contrast, TACI appears to act as an inhibitory receptor (*12*), while the role of BCMA is unclear (*11*).

BR3 is a 184-residue type III transmembrane protein expressed on the surface of B cells (*8*, *9*). The intracellular region bears no sequence similarity to known structural domains or protein−protein interaction motifs. Nevertheless, BAFF-induced signaling through BR3 results in processing of the transcription factor NF-$\kappa$B2/p100 to p52 (*13*, *14*). The extracellular domain (ECD) of BR3 is also divergent. TNFR family members are usually characterized by the presence of multiple cysteine-rich domains (CRDs) in their extracellular region; each CRD is typically composed of ∼40 residues stabilized by six cysteines in three disulfide bonds. Conventional members of this family make contacts with ligand through two CRDs interacting with two distinct patches on the ligand surface (reviewed in ref *15*). However, the BR3 ECD contains only four cysteine residues, capable of forming a partial CRD at most, raising the question of how such a small receptor imparts high-affinity ligand binding. Recent crystal structures show that BAFF indeed adopts the trimeric TNF-like fold (*16*−*18*); however, no structure of any of the BAFF receptors has been described.

Previously we have shown that the BAFF-binding domain of BR3 resides within a 26-residue core region (*14*). Furthermore, we found that six BR3 residues, when structured within a $\beta$-hairpin peptide (bhpBR3), were sufficient to confer BAFF binding and block BR3-mediated signaling. Herein we report the solution structure and alanine-scanning

‡ Data deposition: Coordinates for BR3 and the BAFF−bhpBR3 complex are available from the RCSB Protein Data Bank (PDB ID codes 1OSX and 1OSG, respectively). Resonance assignments for BR3 are available from BMRB (ID code 5750).

* To whom correspondence should be addressed. E-mail: star@gene.com.

⊥ Department of Protein Engineering.

∥ Department of Molecular Oncology.

§ These authors contributed equally to this work.

[1] Abbreviations: BR3, BLyS receptor 3; CRD, cysteine-rich domain; ECD, extracellular domain; TNF, tumor necrosis factor; TNFR, TNF receptor.

10.1021/bi034017g CCC: $25.00 
Published on Web 05/02/2003

mutagenesis of the BR3 ECD. BAFF-interacting residues map to a localized region of BR3, with primary determinants stemming from the six-residue $\beta$-turn. The cocrystal structure of the BAFF−bhpBR3 complex reveals a small surface cavity on BAFF central to receptor binding. Together, these results explain how BR3 recruits binding affinity through such a remarkably focused interaction site.

## EXPERIMENTAL PROCEDURES

*Protein Production.* BR3 ECD was expressed in *Escherichia coli* and purified as previously described (*14*), except that uniformly $^{13}$C-labeled glucose and $^{15}$N-$NH_4Cl$ were substituted in the medium to generate isotopically labeled protein samples for NMR spectroscopy. A PCR-based mutagenesis approach was used to generate D26A and L28A BR3 point mutants; the mutant proteins were expressed and purified as described for the wild-type protein.

For BAFF production, a DNA fragment encoding BAFF residues 82−285 was cloned into the pET15b (Novagen) expression vector, creating a fusion with an N-terminal His-tag followed by a thrombin cleavage site. *E. coli* BL21(DE3) (Novagen) cultures were grown to mid-log phase at 37 °C in LB medium with 50 mg/L carbenicillin and then cooled to 16 °C prior to induction with 1.0 mM IPTG. Cells were harvested by centrifugation after 12 h of further growth and stored at −80 °C. The cell pellet was resuspended in 50 mM Tris, pH 8.0, and 500 mM NaCl and sonicated on ice. After centrifugation, the supernatant was loaded onto a Ni-NTA agarose column (Qiagen). The column was washed with 50 mM Tris, pH 8.0, 500 mM NaCl, and 20 mM imidazole and then eluted with a step gradient in the same buffer with 250 mM imidazole. BAFF-containing fractions were pooled, thrombin was added, and the sample was dialyzed overnight against 20 mM Tris, pH 8.0, and 5 mM $CaCl_2$ at 4 °C. The protein was further purified on a monoQ (Pharmacia) column and finally on an S-200 size exclusion column in 20 mM Tris, 150 mM NaCl, and 5 mM $MgCl_2$.

*Solution Structure of BR3.* NMR spectra were acquired at 20 °C on Bruker DRX-800 or DRX-600 spectrometers equipped with 5-mm inverse $^1$H/$^{15}$N/$^{13}$C triple-resonance probes with three-axis gradient coils. Samples for NMR spectroscopy contained ~1.5 mM BR3, 25 mM $Na_2PO_4$, pH 5.0, 50 mM NaCl, 0.1 mM $NaN_3$, and 0.1 mM DSS-$d_{10}$. The following spectra were recorded using a $^{15}$N-labeled protein sample in 92% $H_2O$/8% $D_2O$: 2D $^1$H−$^{15}$N HSQC, 3D TOCSY−HSQC (mixing times, 33 and 98 ms), 3D HNHA, 3D HNHB, and 3D $^{15}$N NOESY−HSQC (mixing times, 100 and 200 ms) (*19*). $^1$H and $^{15}$N resonance assignments were obtained using conventional NOESY-based methods (*20*). Resonance assignments were completed using a uniformly $^{15}$N/$^{13}$C-labeled protein sample and the following experiments: 2D $^1$H−$^{13}$C HSQC, 3D HNCO, 3D HNCA, 3D CBCA(CO)NH, 3D HCCH−COSY, 3D HCCH−TOCSY, and 3D $^{13}$C NOESY−HSQC (mixing time, 200 ms) (*19*). Stereospecific assignments of methyl groups of Val and Leu residues were obtained using a 15% $^{13}$C-labeled sample (*21*). Distance and dihedral angle restraints were generated as previously described (*22*), except that very strong, strong, medium, weak, and very weak NOE cross-peaks were assigned with upper bound distance restraints of 2.6, 3.0, 4.0, 5.0, and 6.5 Å, respectively. Additional $\phi$ and $\psi$ dihedral angle restraints were derived from $^1$H, $^{15}$N, $^{13}$C′, and $^{13}$C$^\alpha$ chemical shifts using the TALOS program (*23*, *24*). Structures of BR3 were calculated using a simulated annealing protocol with restrained torsion angle dynamics (*25*) using the program XPLOR 98.1 (Accelrys). An ensemble of 20 models with the lowest restraint violation energies represents the solution structure of BR3.

Steady-state $^1$H−$^{15}$N NOEs were measured using pulse sequences described previously (*26*), modified to include $^{15}$N coherence selection via pulsed field gradients (*27*). Individual peak heights were measured from the spectra using FELIX (Accelrys); steady-state NOEs were calculated as the ratios of peak heights in the spectra recorded with (NOE spectrum) and without (no NOE spectrum) proton saturation.

*Library Construction for miniBR3 Shotgun Scanning.* Libraries displaying epitope-tagged miniBR3 on M13 bacteriophage were constructed by successive mutageneses of a previously described phagemid, pW1205a (*28*). This phagemid encodes a peptide epitope tag (MADPNRFRGKDLGG) fused to the N-terminus of human growth hormone followed by M13 gene-8 major coat protein. pW1205a was used as a template for Kunkel mutagenesis (*29*) to generate appropriate templates for miniBR3 shotgun library construction. Oligonucleotides replaced the fragment of pW1205a encoding human growth hormone with DNA fragments encoding a partial sequence of miniBR3 containing TAA stop codons in place of the region to be mutated. The two new templates generated, template 1 (encoding residues 34−42) and template 2 (encoding residues 17−25), were each used to construct a miniBR3 library as previously described (*30*). Each "partial miniBR3" template was used as the template for Kunkel mutagenesis with mutagenic oligonucleotides designed to replace the template stop codons with the complementary region of miniBR3, while simultaneously introducing mutations at the desired sites. At the sites of mutation, wild-type codons were replaced with the corresponding shotgun alanine codon (*28*). Each of these two libraries allowed for mutations at 11 residues in miniBR3 with no mutated positions in common between libraries. Library 1 encoded shotgun codons at positions 17, 18, 20−23, 25, 27, 28, 30, and 33, while library 2 encoded shotgun codons at positions 26, 29, 31, 34, and 36−42. Each library contained $2 \times 10^9$ members, allowing for complete representation of the theoretical diversity ($>10^4$-fold excess).

*Library Sorting and Analysis.* Phage from each of the two libraries described above were subjected to rounds of binding selection against either BAFF (function selection) or an anti-tag antibody (3C8:2F4, Genentech, Inc.) (display selection) immobilized on 96-well Nunc Maxisorp immunoplates. Phage eluted from each target were propagated in *E. coli* XL1-blue; amplified phage were used for selection against the same target as in the previous round. After two rounds of selection, individual clones from each library and selection were grown in a 96-well format in 400 $\mu$L of 2YT medium supplemented with carbenicillin and KO7 helper phage. Supernatants from these cultures were used directly in phage ELISAs to detect phage-displayed variants of miniBR3 capable of binding either BAFF or anti-tag antibody. All clones tested were found to be positive in their respective ELISAs and were then sequenced as previously described (*28*). Sequences of acceptable quality were translated and aligned. For the function selection, 84 and 92 sequences were

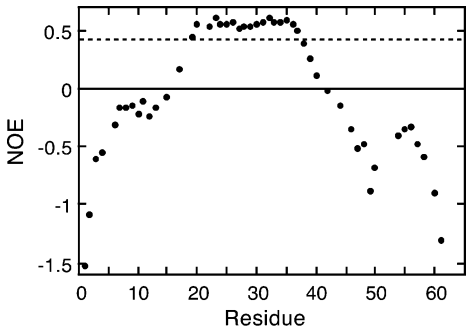


FIGURE 1: $^1H-^{15}N$ heteronuclear NOE values of BR3 plotted as a function of residue number. Absence of a symbol indicates the presence of proline or a residue whose NOE could not be measured due to spectral overlap. Reduced NOE values indicate that these residues are highly mobile in solution relative to the overall rotational tumbling of the molecule. Residues with NOE values above the dotted line represent the ordered portion of BR3 (Cys19-Leu37).

analyzed, while for the display selection, 43 and 45 sequences were analyzed, from libraries 1 and 2, respectively.

*Crystallography.* Crystals of BAFF (82−285) were grown at 19 °C in 3-$\mu$L hanging drops consisting of 2 $\mu$L of protein (9 mg/mL in 50 mM Tris, pH 8.0, and 500 mM NaCl) and 1 $\mu$L of well solution [containing 0.1 M sodium cacodylate, pH 6.7, 19−21% poly(ethylene glycol) (PEG) 3350, and 0.7−1.1 M LiCl]. The space group was determined to be $P6_5$, with two trimers in the asymmetric unit and cell constants of $a = 122$ Å, $c = 157$ Å. Crystals were transferred to a solution containing 28% PEG 3350, 20% glycerol, 80 mM Tris, pH 8.0, 80 mM sodium cacodylate, pH 6.7, and 10 mM bhpBR3 peptide (synthesized as described in ref *14*) and then soaked for 96 h at 19 °C. A 3.0-Å data set of BAFF−bhpBR3 complex was measured at beamline 7-1 at SSRL and processed with HKL (*31*), giving $R_{merge} = 8.1\%$ (41% in the 3.11−3.0 Å shell), 99.6% completeness, 3.5-fold redundancy, and $\langle I/\sigma_I \rangle = 10.5$. The structure was phased by molecular replacement using the BAFF crystal structure (PDB code 1KXG) (*18*) and the program AMoRe (*32*). Good density for all six copies of the peptide was observed in the initial $F_o - F_c$ maps. The solution structure of the peptide (PDB code 1MPV) (*14*) was manually positioned in the density, changes were made to BAFF and to the positions of some of the peptide side chains, and the complex structure was refined with the program REFMAC5 (*32*). NCS restraints were applied to the ligand and peptide (with the exception of BAFF residues 215−226) throughout refinement. The final $R$ factor is 21.3% for 23 768 reflections in the resolution range 30−3.0 Å, with a final $R_{free}$ of 28.6% for 2536 reflections chosen in thin shells throughout the same resolution range. The model has good stereochemistry, with root-mean-square differences in bond lengths and angles of 0.012 Å and 1.36°. The final model consists of two trimers of BAFF residues 142−285 (residues 82−141 are disordered), six copies of the 12-residue bhpBR3 peptide, four $Mg^{2+}$ ions, and 20 water molecules.

## RESULTS

*Solution Structure of BR3.* The structure of the BR3 ECD was examined by NMR spectroscopy. Only the central one-third of the protein adopts a stable fold in solution, as indicated by $^1H-^{15}N$ heteronuclear NOE values (Figure 1).

Table 1. Summary of Structural Statistics for BR3

| | ensemble |
|---|---|
| RMSD from experimental restraints | |
| NOE distance (301)[a] (Å) | 0.0020 ± 0.0007 |
| H-bond (14)[b] (Å) | 0.0067 ± 0.0024 |
| Dihedral (20 $\phi$, 14$\psi$, 12 $\chi_1$) (°) | 0.053 ± 0.020 |
| NOE distance violations | |
| number >0.001 Å | 8.0 ± 2.1 |
| maximum violation (Å) | 0.02 ± 0.01 |
| dihedral angle violations | |
| number >0.01° | 5.2 ± 1.6 |
| maximum violation (°) | 0.34 ± 0.16 |
| RMSD from idealized geometry | |
| bonds (406) (Å) | 0.0014 ± 0.0001 |
| angles (742) (°) | 0.30 ± 0.01 |
| impropers (205) (°) | 0.13 ± 0.01 |
| energies (kcal mol$^{-1}$)[c] | |
| $E_{noe}$ | 0.10 ± 0.05 |
| $E_{cdih}$ | 0.02 ± 0.01 |
| $E_{bond}$ | 0.77 ± 0.12 |
| $E_{angle}$ | 10 ± 1 |
| $E_{improper}$ | 0.54 ± 0.12 |
| $E_{vdW}$ | 6.8 ± 0.9 |

[a] Number of restraints are indicated in parentheses. [b] Each backbone hydrogen bond was restrained using distances of 1.8−2.0 Å for $H^N-O$ and 2.7−3.5 Å for N−O. [c] The final force constants of the target functions used in the simulated annealing protocol were 50 kcal mol$^{-1}$ Å$^{-2}$ for NOE, 300 kcal mol$^{-1}$ rad$^{-2}$ for dihedral angle, 1000 kcal mol$^{-1}$ Å$^{-2}$ for bond lengths, 500 kcal mol$^{-1}$ rad$^{-2}$ for angles and improper dihedrals, and 1 kcal mol$^{-1}$ Å$^{-4}$ for the quartic van der Waals (vdW) repulsion term [hard-sphere effective vdW radii set to 0.80 times their value in the XPLOR parameter set PARMALLH6 (*43*)].

Nineteen residues, including Cys19 through Leu37, define the structured core of the BR3 ECD, while the rest of the N- and C-terminal residues are highly flexible (Figure 1). Previously, the BAFF-binding domain of BR3 was found to reside within a fragment consisting of Thr17-Arg42, denoted miniBR3 (*14*) (Figure 2A). Thus, the structure of BR3 was calculated only for these 26 residues, on the basis of 315 distance and 46 dihedral angle restraints derived from analysis of NMR data collected on the entire BR3 ECD (see Experimental Procedures; Table 1). The ordered residues are well-defined by the data and have good covalent geometry [92.6% of the residues are in the most favored or allowed regions of $\phi\psi$ space (*33*)].

The core of the structure consists of two $\beta$-strands (residues 23−26 and 31−34) linked by a type I $\beta$-turn (residues 27−30), forming a hairpin connected by a disulfide bond between Cys24 and Cys35. The hairpin is tethered to the N-terminal region by a second disulfide between Cys32 and Cys19 (Figure 2B,C). The structure is analogous to the first half of a canonical CRD and adopts an A-like module fold (*34*) (Figure 2D). Typical A1 modules are characterized by having an aromatic residue five residues after the first cysteine [see Figure 2D (*34*)]. In BR3, Cys24 occupies this position, forming a disulfide bond with Cys35. The loop contained within the A module is highly variable in length, composition, and structure among TNFR CRDs, yet it provides many of the contact residues in both the lymphotoxin-TNFR1 and Apo2L/TRAIL-DR5 complexes (*35*−*38*). In BR3, this loop encompasses six residues, Asp26-His31, and adopts a type I $\beta$-turn centered at Leu28/Val29.

*Mutational Analysis of miniBR3.* Given that the BAFF-binding affinity of the 26-residue miniBR3 is equivalent to that of the entire BR3 ECD (*14*), shotgun alanine scanning (*28*) of miniBR3 was used to rapidly obtain information on

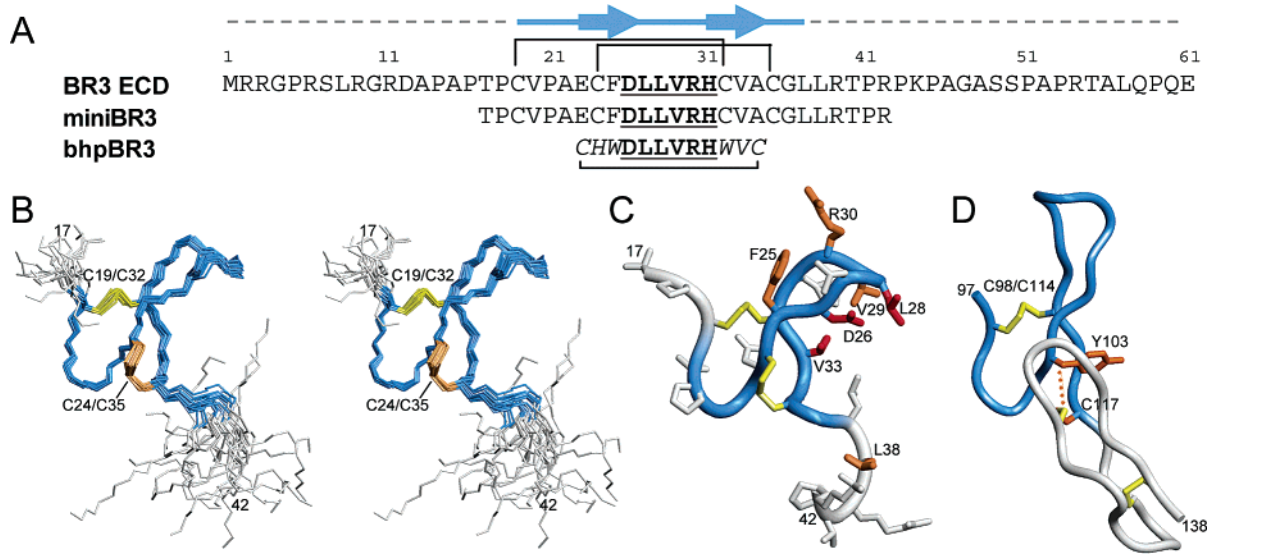


FIGURE 2: Sequence and structure of the BR3 ECD. (A) Sequence of BR3 variants used in this study. The secondary structure of the ordered region of BR3 is indicated above (in blue); dashed lines mark the flexible portion of the BR3 ECD. (B) Stereoview of the ensemble of 20 BR3 models shown superposed using backbone atoms of residues 20−36. The RMSD with respect to the mean coordinates for this superposition is 0.36 ± 0.09 Å for the backbone atoms and 0.84 ± 0.11 Å for all heavy atoms. The ordered region based on $^{1}H-^{15}N$ NOE values is colored blue. (C) Representative structure of BR3. Important BAFF-binding determinants based on shotgun alanine scanning are labeled and colored (red, wild-type residue found exclusively; orange, $F > 10$, Table 2). (D) Structure of a canonical CRD, CRD3 of TNFR1 [PDB code 1TNR (*35*)]. The region with topology similar to that of BR3 is indicated in blue; the A1 module is contained within this region but does not include Cys117. Canonical disulfide bonds are shown in yellow; the noncanonical disulfide of BR3 connects the two side-chain positions shown in orange. Note that the binding loop of TNFR1 shown at the "top" of the module has a three-residue insertion relative to BR3. Like the BR3 loop, this loop adopts a hairpin structure, but unlike the BR3 loop, the tip of the turn points in the opposite direction and does not contact lymphotoxin in the ligand−receptor complex (*35*).

the contribution to ligand binding of individual BR3 residues. Two phage display libraries were constructed, each having mutations at 11 positions. Wild-type codons were replaced by degenerate codons, allowing residues to vary as the wild-type amino acid or alanine. For some residues in miniBR3 (Phe, Leu, Arg, and His), the shotgun codon allows two additional amino acid substitutions. In addition, alanine was allowed to vary as glycine. Together these libraries contain mutations of every residue in miniBR3, excluding the four cysteines. Each of the miniBR3 shotgun alanine libraries was subjected to two different selections: selection for binding the ligand, BAFF (function selection), and selection for binding an antibody (*39*) that recognizes an epitope tag N-terminally displayed on all miniBR3 library members (display selection). The display selection was included in order to normalize the BAFF-binding selection for expression differences between library members. After two rounds of sorting, positive clones were identified and sequenced. The number of times a particular amino acid was found at each position, and the normalized wild-type/mutant functional ratio, *F*, are shown in Table 2.

As discussed previously (*39*), *F* values describe the effect of mutation on target binding, while accounting for differences in display efficiencies, with values >1 representing deleterious mutations and those <1 representing favorable mutations. Given the relatively small number of sequences analyzed (see Experimental Procedures), only those mutations that showed a greater than 10-fold effect (i.e., $F > 10$ or $F < 0.1$) are considered statistically significant. For 7 out of 20 non-alanine residues, mutation to alanine resulted in a significant decrease in BAFF binding ($F > 10$, Table 2, Figure 2C). For three of these residues, Asp26, Leu28, and Val33, only the wild-type amino acid was observed in the BAFF-binding selection, suggesting that they are each very important for ligand binding.

Table 2: Shotgun Alanine Scan of BR3[a]

| | BAFF selection | | | | display selection | | | | *F* | | |
|---|---|---|---|---|---|---|---|---|---|---|---|
| residue | wt | Ala | m2 | m3 | wt | Ala | m2 | m3 | Ala | m2 | m3 |
| Thr17 | 36 | 48 | | | 19 | 24 | | | 0.95 | | |
| Pro18 | 35 | 49 | | | 19 | 24 | | | 0.90 | | |
| Val20 | 52 | 32 | | | 23 | 20 | | | 1.4 | | |
| Pro21 | 17 | 67 | | | 14 | 28 | | | 0.51 | | |
| Ala22 | 20 | | $64^{G}$ | | 13 | | 29 | | | 0.70 | |
| Glu23 | 78 | 5 | | | 32 | 11 | | | 5.4 | | |
| Phe25 | 74 | 3 | $1^{S}$ | $6^{V}$ | 8 | 15 | 14 | 6 | **46** | **130** | 9.3 |
| Asp26 | 92 | 0 | | | 38 | 7 | | | **>17** | | |
| Leu27 | 0 | 3 | $81^{P}$ | $0^{V}$ | 2 | 19 | 14 | 8 | <9.5 | **<0.09** | nd[b] |
| Leu28 | 84 | 0 | $0^{P}$ | $0^{V}$ | 6 | 15 | 15 | 7 | **>210** | **>210** | **>98** |
| Val29 | 85 | 3 | | | 15 | 30 | | | **57** | | |
| Arg30 | 19 | 3 | $62^{G}$ | $0^{P}$ | 5 | 13 | 20 | 4 | **17** | 1.2 | **>15** |
| His31 | 6 | 41 | $44^{D}$ | $0^{P}$ | 5 | 10 | 24 | 6 | 0.29 | 0.66 | >7 |
| Val33 | 84 | 0 | | | 19 | 24 | | | **>110** | | |
| Ala34 | 76 | | $11^{G}$ | | 9 | | 36 | | | **28** | |
| Gly36 | 68 | 24 | | | 31 | 14 | | | 1.3 | | |
| Leu37 | 49 | 27 | $2^{P}$ | $14^{V}$ | 6 | 18 | 12 | 9 | 5.4 | **49** | 5.3 |
| Leu38 | 72 | 4 | $6^{P}$ | $10^{V}$ | 8 | 21 | 8 | 8 | **47** | **12** | 7.2 |
| Arg39 | 34 | 11 | $43^{G}$ | $4^{P}$ | 9 | 12 | 18 | 6 | 4.1 | 1.6 | 5.7 |
| Thr40 | 27 | 65 | | | 21 | 24 | | | 0.48 | | |
| Pro41 | 42 | 50 | | | 14 | 31 | | | 1.9 | | |
| Arg42 | 13 | 12 | $54^{G}$ | $13^{P}$ | 7 | 10 | 25 | 2 | 1.6 | 0.86 | 0.29 |

[a] The occurrence of the wild-type residue (wt) or each mutation (Ala, m2, m3) found among sequenced clones following two rounds of selection for binding to BAFF (function selection) or anti-tag antibody (display selection) is shown for each scanned position in miniBR3. The occurrence of the wild-type residue was divided by that of the mutant to determine a wt/mutant ratio for each mutation at each position (not shown). A normalized frequency ratio (*F*) was calculated to quantify the effect of each mutation on BAFF-binding while accounting for display efficiencies: i.e., $F = [\text{wt/mutant(BAFF selection)}] \div [\text{wt/mutant(display selection)}]$. Deleterious mutations have ratios >1, while advantageous mutations have ratios <1; boldface indicates a >10-fold effect. *F* values calculated for Asp26, Leu28, and Val33 represent a lower limit since Ala was not observed at these sites in the BAFF selection. Alternative residues from the shotgun code are shown as m2 and m3, with the amino acid identity shown using single-letter code in superscript. [b] Neither leucine nor m3(V) was observed at this position.

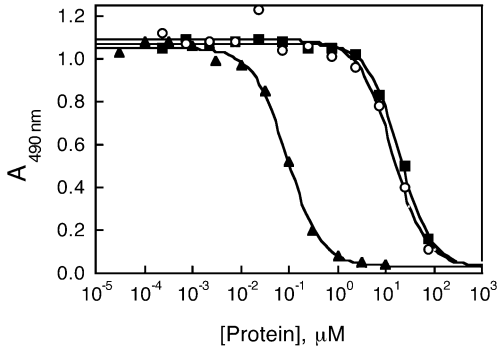


FIGURE 3: Competitive displacement of biotinylated miniBR3 binding to BAFF. (ELISA performed and analyzed as described in ref *14*). Data are for BR3 ECD (filled triangles) and two corresponding point mutants, D26A (filled squares) and L28A (open circles); $IC_{50}$ values derived from the fitted curves are 92 nM, 20 $\mu$M, and 14 $\mu$M, respectively.

Deleterious effects on binding, as measured by shotgun alanine scanning, could result directly from loss of an important side-chain contact or indirectly from affecting the folding efficiency or structure of the protein on phage. For example, Arg30 in BR3 adopts a positive $\phi$ value that is necessary for accommodating a type I $\beta$-turn conformation in a $\beta$-hairpin. This conformation is not readily adopted by alanine (*40*) or arginine; however, it would be accommodated by glycine [which is selected as frequently as arginine ($F$ = 1.2)] and would not be tolerated at all by proline ($F$ > 15; Table 2). These results suggest that maintenance of the turn structure is important, and also that the arginine side chain contributes favorable interactions with BAFF. Similarly, alanine or serine substitution of Phe25, located in the non-hydrogen-bonded position of the $\beta$-hairpin, likely destabilizes the $\beta$-hairpin structure (*41*) and thus could indirectly influence contributions of the turn residues onto which Phe25 packs. Interestingly, proline was selected in place of Leu27 nearly exclusively. Given that there is a statistical preference for proline in this position of a type I $\beta$-turn (*42*), Pro27 may stabilize the turn structure, further emphasizing the importance of this turn conformation in promoting BAFF binding.

To obtain a direct measure of the effect of alanine substitution of Asp26 and Leu28 on BAFF binding, purified mutant proteins were generated in the full BR3 ECD and assayed in a competitive displacement ELISA (*14*) (Figure 3). In this assay, BR3 ECD and miniBR3 displayed equivalent affinities for BAFF (*14*). The assay shown in Figure 3 resulted in an $IC_{50}$ value for BR3 ECD of 92 nM, which compares favorably with a $K_d$ of 30 $\pm$ 10 nM determined for BR3 ECD binding to BAFF measured using isothermal titration calorimetry (R. Kelley, unpublished results). In contrast, the mutant protein D26A showed a 20 $\mu$M $IC_{50}$, indicating a 210-fold decrease in binding relative to wild-type BR3. Similarly, L28A exhibited a 150-fold decrease in BAFF binding (14 $\mu$M $IC_{50}$). These data, in conjunction with the shotgun scan results, highlight the importance of these residues for high-affinity BAFF binding. In addition, these results suggest that $F$ values calculated for these sites reflect binding interactions and not folding efficiencies on phage.

*BAFF−bhpBR3 Complex.* We have previously shown that six BR3 loop residues, $^{26}$DLLVRH$^{31}$, structured by a $\beta$-hairpin scaffold, are sufficient to bind BAFF and block BR3 binding (15 $\mu$M $IC_{50}$) (*14*). These six residues include four of the seven residues that show a >10-fold effect on binding when substituted by alanine (Table 2). A comparison of the solution structures of BR3 and bhpBR3 shows that the $\beta$-hairpin scaffold faithfully presents the BR3 turn, with a backbone root-mean-square deviation (RMSD) between the mean coordinates of the two ensembles of 0.34 Å, within the uncertainty of the structure determinations (Figure 4A). Thus, structural analysis of how BAFF interacts with BR3 loop residues in the context of the hairpin peptide should reflect interactions of the same residues in the context of the full BR3 protein.

The 3.0-Å crystal structure of the bhpBR3 peptide in complex with BAFF shows that the hairpin structure of the

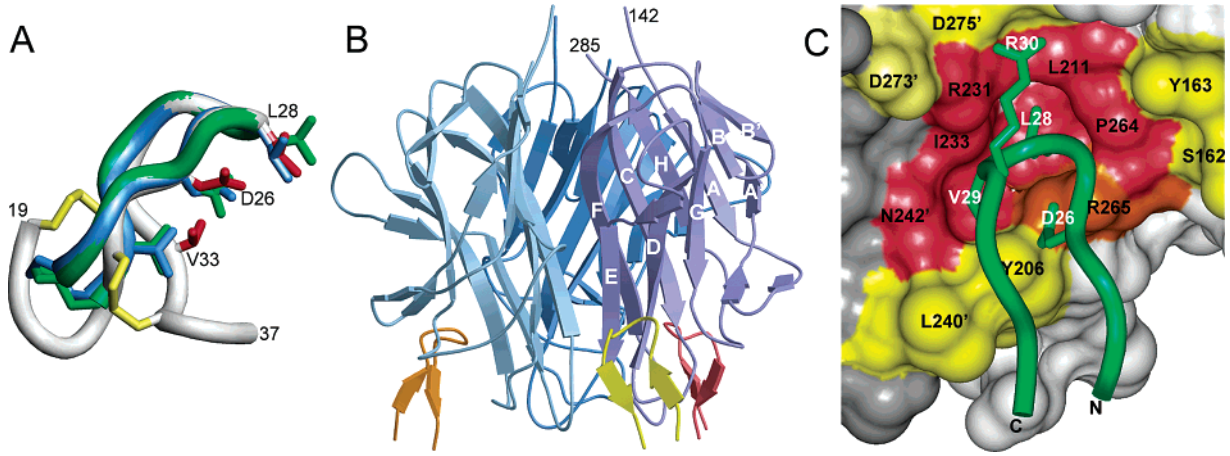


FIGURE 4: Crystal structure of BAFF−bhpBR3 complex. (A) Structural comparison of free (blue; PDB 1MPV) and ligand-bound (green) bhpBR3 with free BR3 (white). Only side chains of Asp26, Leu28, Val33, and the cysteine residues are shown. Note the excellent agreement in turn conformation between peptide and protein; also note that, while there is a valine residue at the position analogous to Val33 in the sequence of the bhpBR3 peptide (Figure 1A), it is located in a different position in space in the peptide compared to the protein structure and is not well-ordered in the electron density of the BAFF−peptide complex (see text). (B) Overall view of BAFF−bhpBR3 complex. The BAFF trimer is shown in shades of blue, the peptide in shades of orange. (C) Close-up of the BAFF−bhpBR3 interface. The BAFF surface is colored on the basis of the percentage of surface area buried upon complex formation (red, 75−100%; orange, 50−74%; dark yellow, 25−49%; light yellow, 1−24%). BAFF and peptide residues are labeled in black and white, respectively. In this view, Ala207 and Gly209 of BAFF are located directly below Val29 and Leu28 of bhpBR3, respectively. Side chains of only the four BR3 turn residues implicated to be important for BAFF binding by the BR3 ECD are shown (Table 2).

peptide is maintained in the complex (Figure 4). The main-chain conformation of the entire peptide is unambiguous in the electron density, and hairpin scaffold side chains Cys23, Trp25, Trp32, and Cys34 are well-ordered. However, the side-chain conformations of the other scaffold residues, His24 and Val33, as well as the BR3 turn residues Leu27 and His31 are not well-defined past the C$\beta$ atoms in the electron density.

Three copies of the bhpBR3 peptide bind one BAFF trimer, each occupying a pocket on the BAFF surface located at the monomer−monomer interface (Figure 4B,C). The base of the pocket is lined by residues of strand D, Ala207 and Gly209, whose lack of side chain is responsible for the cavity on the ligand surface. The pocket is bordered by the side chains of Ser162, Tyr163, Tyr206, Leu211, Arg231, Ile233, Pro264, and Arg265 from one monomer and Leu240′, Asn242′, Asp273′, and Asp275′ from the adjacent monomer. In total, the BAFF−bhpBR3 complex buries approximately 840 Å$^2$ of surface area, of which 370 Å$^2$ is buried by BAFF and 470 Å$^2$ by the peptide (440 Å$^2$ of which comes from the six BR3 turn residues). Asp26, Leu28, and Val29 are the most buried peptide residues. Asp26 forms a salt bridge to Arg265 and a hydrogen bond to the hydroxyl group of Tyr206 on BAFF. The interface is centered around Leu28 that lies fully buried in the cavity lined by Gly209. In addition, the carbonyl of Leu28 makes a hydrogen bond to BAFF residue Arg231. Val29 is buried in a shallow pocket adjacent to the Leu28 binding site. Two carboxylate groups on the BAFF surface, Asp273′ and Asp275′, are proximal to the side chain of Arg30 from the peptide, although no direct salt bridge is observed.

## DISCUSSION

*BAFF−BR3 Interactions.* The excellent correspondence between the contacts seen in the BAFF−bhpBR3 peptide complex and the mutational analysis of the BR3 protein permits docking of the ordered portion of the BR3 receptor onto the ligand to identify other potential interactions. With BR3 turn residues $^{26}$DLLVRH$^{31}$ occupying the same position on BAFF as seen here for the peptide complex, Val33 would then pack against Tyr206, thereby accounting for the importance of this valine indicated by alanine mutation. The other key BR3 residue outside the turn implicated in BAFF binding, Leu38 (Table 2), is not well-ordered in the absence of ligand (Figure 1A). Nevertheless, this region of BR3 could wrap around the BAFF surface in the complex, providing additional hydrophobic contacts. The fact that bhpBR3 is missing the contributions provided by Val33 and Leu38 in the context of the BR3 ECD likely accounts for the observation that the peptide binds BAFF 200-fold more weakly than the protein (*14*). The flexible N- and C-terminal BR3 residues outside the 26-residue miniBR3 core would likely be positioned away from the ligand surface and thus are not predicted to interact with BAFF, consistent with the observation that miniBR3 has the same affinity for BAFF as the full-length ECD (*14*).

*Implications for TACI and BCMA Binding to BAFF and APRIL.* TACI and BCMA contain sequences homologous to the BR3 turn in the predicted binding loops of their respective CRDs (DSLLHA, DPLLGT, and DHLLRD for BCMA and CRDs 1 and 2 of TACI, respectively). The key roles that Asp26 and Leu28 of BR3 play at the ligand−receptor interface suggest that the conserved aspartic acid and leucine residues (underlined above) participate in similar interactions in both the BAFF−BCMA and BAFF−TACI complexes. Although the other loop residues vary, all of these six-residue sequences are predicted to adopt a turn conformation similar to that seen here for BR3. In fact, three of the residues that differ among these BAFF receptor loop sequences were also not conserved in the BR3 variants selected for BAFF binding (Table 2), indicating that they are not essential for ligand binding and might produce improved affinity when substituted.

Unlike BR3, TACI and BCMA also bind the homologous TNF-like ligand APRIL. APRIL is expected to have a similar cavity on its surface, with the positions analogous to Gly209, Ile233, Pro264, and Arg265 being conserved; however, substitution of other residues bordering the pocket could account for differences in the observed receptor-binding specificity. For example, Y206F and A207T (BAFF numbering is used to highlight APRIL sequence differences) will change the hydrogen-bonding between ligand and Asp26 of the receptor; L240′R and N242′Y will change the Val29 pocket, which would be occupied by a leucine in both TACI and BCMA; and D273′S and D275′H will likely affect interactions with receptor residues in the position of Arg30. Therefore, interactions with the receptor DxL motif should be very similar in BAFF− and APRIL−receptor complexes, but differing peripheral interactions will modulate binding affinity and specificity.

*Comparison with Other TNF−TNFR Complexes.* The complex of BAFF bound to a peptide derived from BR3 defines the primary receptor-binding site on BAFF. This site is analogous to the sites used by CRD3 of TNFR1 or DR5 in binding their cognate ligands, lymphotoxin and Apo2L/TRAIL (*35*−*38*). Each of these interaction sites is centered around residues from strand D of one ligand monomer and includes adjacent residues from neighboring strands. For instance, Ala207 of BAFF is in the position analogous to Gln205 of Apo2L/TRAIL and Tyr106 of lymphotoxin (*16*); each of these residues makes key interactions in its respective complex. In all three cases, this interaction area is located at the monomer−monomer interface of the ligand trimer. Of course, in the BAFF−BR3 complex, this site represents the entire ligand−receptor interface, whereas in the other two complexes, this region encompasses only half of the ligand−receptor interface, with CRD2 of each receptor contributing substantial additional contacts. Significantly, in neither case are there surface cavities on the ligand that are utilized for receptor binding.

The finding that BR3 utilizes such a localized epitope for binding a surface cavity on BAFF has important therapeutic implications. BAFF antagonists could have great therapeutic potential for the treatment of a variety of autoimmune diseases (*1*). The results presented here suggest that small molecules might intervene effectively and be useful in blocking BR3-mediated signaling events.

## ACKNOWLEDGMENT

We thank S. S. Sidhu for advice about miniBR3 library design and shotgun scanning; S. Leung for BAFF fermentation; C. Wiesmann for advice on peptide soaking conditions; M. Franklin, M. Ultsch, and the beamline staff at SSRL 7-1

for assistance with synchrotron data collection; members of the mass spectrometry, protein sequencing, and DNA sequencing groups at Genentech; and N. J. Skelton and A. M. de Vos for many helpful discussions.

## REFERENCES


1. Mackay, F., and Browning, J. L. (2002) *Nature Rev. Immunol. 2*, 465−475.
2. Mackay, F., Woodcock, S. A., Lawton, P., Ambrose, C., Baetscher, M., Schneider, P., Tschopp, J., and Browning, J. L. (1999) *J. Exp. Med. 190*, 1697−1710.
3. Gross, J. A., Johnston, J., Mudri, S., Enselman, R., Dillon, S. R., Madden, K., Xu, W., Parrish-Novak, J., Foster, D., Lofton-Day, C., Moore, M., Littau, A., Grossman, A., Haugen, H., Foley, K., Blumberg, H., Harrison, K., Kindsvogel, W., and Clegg, C. H. (2000) *Nature 404*, 995−999.
4. Khare, S. D., Sarosi, I., Xia, X.-Z., McCabe, S., Miner, K., Solovyev, I., Hawkins, N., Kelley, M., Chang, D., Van, G., Ross, L., Delaney, J., Wang, L., Lacey, D., Boyle, W. J., and Hsu, H. (2000) *Proc. Natl. Acad. Sci. U.S.A. 97*, 3370−3375.
5. Cheema, G. S., Roschke, V., Hilbert, D. M., and Stohl, W. (2001) *Arthritis Rheum. 44*, 1313−1319.
6. Groom, J., Kalled, S. L., Cutler, A. H., Olson, C., Woodcock, S. A., Schneider, P., Tschopp, J., Cachero, T. G., Batten, M., Wheway, J., Mauri, D., Cavill, D., Gordon, T. P., Mackay, C. R., and Mackay, F. (2002) *J. Clin. Invest. 109*, 59−68.
7. Zhang, J., Roschke, V., Baker, K. P., Wang, Z., Alarcon, G. S., Fessler, B. J., Bastian, H., Kimberly, R. P., and Zhou, T. (2001) *J. Immunol. 166*, 6−10.
8. Thompson, J. S., Bixler, S. A., Qian, F., Vora, K., Scott, M. L., Cachero, T. G., Hession, C., Schneider, P., Sizing, I. D., Mullen, C., Strauch, K., Zafari, M., Benjamin, C. D., Tschopp, J., Browning, J. L., and Ambrose, C. (2001) *Science 293*, 2108−2111.
9. Yan, M., Brady, J. R., Chan, B., Lee, W. P., Hsu, B., Harless, S., Cancro, M., Grewal, I. S., and Dixit, V. M. (2001) *Curr. Biol. 11*, 1547−1552.
10. Yan, M., Marsters, S. A., Grewal, I. S., Wang, H., Ashkenazi, A., and Dixit, V. M. (2000) *Nat. Immunol. 1*, 37−41.
11. Schiemann, B., Gommerman, J. L., Vora, K., Cachero, T. G., Shulga-Morskaya, S., Dobles, M., Frew, E., and Scott, M. L. (2001) *Science 293*, 2111−2114.
12. Yan, M., Wang, H., Chan, B., Roose-Girma, M., Erickson, S., Baker, T., Tumas, D., Grewal, I. S., and Dixit, V. M. (2001) *Nat. Immunol. 2*, 638−643.
13. Claudio, E., Brown, K., Park, S., Wang, H., and Siebenlist, U. (2002) *Nat. Immunol. 3*, 958−965.
14. Kayagaki, N., Yan, M., Seshasayee, D., Wang, H., Lee, W., French, D. M., Grewal, I. S., Cochran, A. G., Gordon, N. C., Yin, J., Starovasnik, M. A., and Dixit, V. M. (2002) *Immunity 10*, 515−524.
15. Bodmer, J.-L., Schneider, P., and Tschopp, J. (2002) *Trends Biochem. Sci. 27*, 19−26.
16. Karpusas, M., Cachero, T. G., Qian, F., Boriack-Sjodin, A., Mullen, C., Strauch, K., Hsu, Y.-M., and Kalled, S. L. (2002) *J. Mol. Biol. 315*, 1145−1154.
17. Liu, Y., Xu, L., Opalka, N., Kappler, J., Shu, H.-B., and Zhang, G. (2002) *Cell 108*, 383−394.
18. Oren, D. A., Li, Y., Volovik, Y., Morris, T. S., Dharia, C., Das, K., Galperina, O., Gentz, R., and Arnold, E. (2002) *Nat. Struct. Biol. 9*, 288−292.
19. Cavanagh, J., Fairbrother, W. J., Palmer, A. G., III, and Skelton, N. J. (1995) *Protein NMR Spectroscopy: Principles and Practice*, Academic Press, San Diego.
20. Wüthrich, K. (1986) *NMR of Proteins and Nucleic Acids*, J. Wiley and Sons, New York.
21. Neri, D., Szyperski, T., Otting, G., Senn, H., and Wüthrich, K. (1989) *Biochemistry 28*, 7510−7516.
22. Fairbrother, W. J., Champe, M. A., Christinger, H. W., Keyt, B. A., and Starovasnik, M. A. (1998) *Structure 6*, 637−648.
23. Cornilescu, G., Delaglio, F., and Bax, A. (1999) *J. Biomol. NMR 13*, 289−302.
24. Pan, B., Li, B., Russell, S. J., Tom, J. Y. K., Cochran, A. G., and Fairbrother, W. J. (2002) *J. Mol. Biol. 316*, 769−787.
25. Stein, E. G., Rice, L. M., and Brünger, A. T. (1997) *J. Magn. Reson. 124*, 154−164.
26. Skelton, N. J., Akke, M., Kördel, J., Palmer, A. G. P., Rance, M., and Chazin, W. J. (1993) *J. Magn. Reson. B 102*, 253−264.
27. Muhandiram, D. R., and Kay, L. E. (1994) *J. Magn. Reson. B 103*, 203-216.
28. Weiss, G. A., Watanabe, C. K., Zhong, A., Goddard, A., and Sidhu, S. S. (2000) *Proc. Natl. Acad. Sci. U.S.A. 97*, 8950−8954.
29. Kunkel, T. A., Roberts, J. D., and Zakour, R. A. (1987) *Methods Enzymol. 154*, 367−382.
30. Sidhu, S. S., Lowman, H. B., Cunningham, B. C., and Wells, J. A. (2000) *Methods Enzymol. 328*, 333−363.
31. Otwinowski, Z., and Minor, W. (1997) *Methods Enzymol. 176*, 307−326.
32. CCP4. (1994) *Acta Crystallogr. D 50*, 760−763.
33. Laskowski, R. A., Rullman, J. A. C., MacArthur, M. W., Kaptein, R., and Thornton, J. M. (1996) *J. Biolmol. NMR 8*, 477−486.
34. Naismith, J. H., and Sprang, S. R. (1998) *Trends Biochem. Sci. 23*, 74−79.
35. Banner, D. W., D'Arcy, A., Janes, W., Gentz, R., Schoenfeld, H.-J., Broger, C., Loetscher, H., and Lesslauer, W. (1993) *Cell 73*, 431−445.
36. Hymowitz, S. G., Christinger, H. W., Fuh, G., Ultsch, M., O'Connell, M., Kelley, R. F., Ashkenazi, A., and de Vos, A. M. (1999) *Mol. Cell 4*, 563−571.
37. Cha, S.-S., Sung, B.-J., Kim, Y.-A., Song, Y.-L., Kim, H.-J., Kim, S., Lee, M.-S., and Oh, B.-H. (2000) *J. Biol. Chem. 275*, 31171−31177.
38. Mongkolsapaya, J., Grimes, J. M., Chen, N., Xu, X.-N., Stuart, D. I., Jones, E. Y., and Screaton, G. R. (1999) *Nat. Struct. Biol. 6*, 1048−1053.
39. Skelton, N. J., Koehler, M. F. T., Zobel, K., Wong, W. L., Yeh, S., Pisabarro, M. T., Yin, J., Lasky, L. A., and Sidhu, S. S. (2003) *J. Biol. Chem. 278*, 7645−7654.
40. Nakamura, G. R., Starovasnik, M. A., Reynolds, M. E., and Lowman, H. B. (2001) *Biochemistry 40*, 9828−9835.
41. Cochran, A. G., Tong, R. Y., Starovasnik, M. A., Park, E. J., McDowell, R. S., Theaker, J. E., and Skelton, N. J. (2001) *J. Am. Chem. Soc. 123*, 625−632.
42. Hutchinson, E. G., and Thornton, J. A. (1994) *Protein Sci. 3*, 2207−2216.


BI034017G